JOURNAL OF MATERIALS SCIENCE 29 (1994) 1686–1691

Coarsening and properties of extruded Al–8Fe–4Ni–1Mo alloys

G. SHAO, A. P. MIODOWNIK
Department of Materials Science and Engineering, University of Surrey, Guildford Surrey GU2 5XH, UK

H. MCSHANE
Department of Materials, Imperial College, London SW7, UK

G. SCHARF
Vereinigte Aluminium Worke D5300 Bonn 1, Germany

Characterization of rapidly solidified Al–8Fe–4Ni–1Mo alloy shows that subsequent extrusion generates a non-uniform microstructure which may be attributed to the non-uniform deformation during extrusion. The mechanical properties were found to be closely related to the extrusion ratio. It is believed that the degradation of the microstructure is due to the severe deformation during processing, and hence a compromise is needed between optimum powder bonding and the lowest extent of deformation in the consolidation process.

1. Introduction

The development of aluminium alloys containing transitional metal elements for elevated temperature application has been of continuing interest in the field of materials science and engineering. Following the initial rapid solidification processing work of Jones, alloys based on Al–Fe–X have emerged as potential candidates for elevated temperature application [1–5]. The Al–Fe–Ni system at the Al-rich corner has been of fundamental and practical interest as the ternary phase (τ) based on $Al_9(FeNi)_2$ is very effective in increasing the modulus of the alloys because of its larger aluminium/transitional metal ratio [6–8]. Also, τ is a stable phase resistant to shear [7, 8]. The wide range of stoichiometry of τ and its strong orientation relationship with α-Al can also lead to optimum coherence and enhanced thermal stability of Al–Fe–Ni alloys [9].

Prior investigations of rapidly solidified Al–Fe–Ni alloys have largely been concerned with alloys where the Fe/Ni ratio is $\leqslant 1$. Boettinger *et al.* [10] investigated the microstructure of an Al–3.7 wt % Ni–1.5 wt % Fe alloy prepared by melt spinning and electron-beam surface melting. Kim & Jackson reported orientation relationship in a hot pressed Al–6Fe–6Ni powders [11], while the investigations by Premkumar *et al.* were largely on the mechanical properties of Al–5Fe–5Ni powder extrusions [7, 8]. The solidification process of the alloy powders have been reported previously [12]. This study concentrates on the microstructural development of alloy powders during extrusion, and hence the microstructure and property relationship of rapid solidification processing of Al–Fe–Ni–Mo extrusions.

2. Experimental procedure

Alloy powders were supplied by Alpoco under Euram contract MAIE/0076/C. Extrusions of sub-45 μm high-pressure Ar-atomized Al–8% Fe–4% Ni–1 wt% Mo alloy powder were prepared with different extrusion ratios, i.e. 5:1 (extrusion A) and 27:1 (extrusion B) [13]. Transmission electron microscopy (TEM) specimens of alloy powders were prepared by copper plating and followed by ion-beam thinning [12]. Thin foils of alloy extrusions for TEM study were prepared by initial electrolytic polishing and completed by ion-beam thinning. Electron microscopy was conducted on a Philips EM 400T with a Link AN10000 EDX system and JEOL 2000-fx transmission electron microscopes, as well as a Cambridge S250 scanning electron microscope (SEM). X-ray diffraction (XRD) analysis was also used for phase identification with monochromatic CuK_α radiation.

3. Results

3.1. Powder microstructure

XRD revealed that powder particles below 200 μm in diameter were composed only of α-Al and τ phases. There was no evidence of the Al_6Fe, Al_3Fe, or Al_xMo phases. Both the peak position and the relative peak intensities of the τ phase were close to those of Al_9Co_2, as shown in Table I. The crystal structure of the τ phase was thus determined to be isomorphous with Al_9Co_2 with $a = 0.86464$ nm, $b = 0.6370$ nm, $c = 0.62612$ nm and $\beta = 95°$ when the particle size was larger than 80 μm. The amount of the τ phase in the powder particles decreased with particle size, as

0022–2461

TABLE I X-ray diffraction data

hkl	τ, Kim [11]	Al_9Co_2, ASTM		Extrusion		Powder of different size ranges					
		d(nm)	Int. (I)	d(nm)	Int. (I)	80–200 μm		25–45 μm		< 25 μm	
						d(nm)	Int. (I)	d(nm)	Int. (I)	d(nm)	Int. (I)
001	–	0.6102	5	0.6226	4	0.6237	2	–	–	–	–
110	0.5110	0.5062	74	0.5111	62	0.5122	57	0.5113	68	0.5110	57
011	0.4450	0.4380	100	0.4445	100	0.4452	100	0.4451	100	0.4446	100
200	–	0.4263	18	0.4304	18	0.4306	14	0.4302	18	0.4296	20
$\bar{1}11$	0.4050	0.3994	80	0.4050	81	0.4056	71	0.4055	82	0.4051	80
111	0.3865	0.3805	87	0.3853	87	0.3859	86	0.3854	93	0.3851	93
$\bar{2}01$	0.3705	0.3640	49	0.3686	49	0.3689	46	0.3689	50	0.3689	53
210	0.3520	0.3529	62	0.3558	68	0.3561	68	0.3560	71	0.3557	70
201	0.3398	0.3366	39	0.3402	34	0.3406	36	0.3403	39	0.3399	43
$\bar{2}11$	–	0.3150	6	0.3187	3	0.3189	5	–	–	–	–
002	0.3097	0.3051	35	0.3104	39	0.3111	36	0.3114	34	0.3111	33
120	0.2953	0.2951	38	0.2975	40	0.2980	38	0.2976	43	0.2974	37
021	–	0.2796	3	0.2827	7	0.2827	4	0.2827	5	–	–
310	–	0.2590	18	0.2714	14	0.2724	14	0.2718	14	0.2716	13
$\bar{3}02$	0.2606	0.2585	21	0.2596	49	0.2598	48	0.2599	55	0.2596	53
112	–	0.2558	22	–	–	–	–	–	–	–	–

shown through changes in the intensity ratio $I_\tau/I_{\alpha\text{-Al}(1\,1\,1)}$ (Table I).

Optical microscopy showed that the powder microstructure was markedly dependent on the powder size. The larger the powder particle, the more nucleation sites it contained and the coarser the microstructure, as shown in Fig. 1 . Powders in the size range of 8–20 μm usually had a two-zone microstructure, zones A and B, as indicated in Fig. 2. Nucleants can be distinguished in the larger powder particles which are totally composed of zone B structure.

Fig. 2 shows the microstructure of a powder particle around 8 μm in diameter. The matrix consists of a single α-Al crystal, and solidification was nucleated inside the powder particle. The microcellular structure of α-Al becomes coarser with increasing distance from the nucleation site towards the particle surface. The selected area diffraction pattern (SADP) from area 1 in Fig. 2a showed all the 24 equivalent orientation variants between α-Al matrix and τ (Fig. 2c). At the nucleation site (site 1 in Fig. 2a), the fine intercellular τ precipitates are isolated from each other (Fig. 2b). However, some of the orientation variants disappeared and a new dominant orientation variant was present at site 2 where the intercellular τ precipitates became coarser and more continuous. The dominant orientation pair was determined from the double diffraction spots in Fig. 2d, as (1 1 1)α-Al/(2 0 1)τ.

Fig. 3a shows the typical microstructure of the 45 μm powder particles. It is totally composed of coupled (α-Al + τ) eutectic and primary τ. Electron diffraction analysis shows that both the primary τ and the eutectic τ have the same orientation. It is therefore concluded that the nucleants in the optical micrograph (Fig. 2) are primary τ particles. CBED patterns from the eutectic τ phase are shown in Fig. 3b and c. The τ lattice parameters derived from these are in good agreement with (and the relative intensities of the diffraction discs are comparable to) the results of XRD (Table I). The composition of the τ phase in the

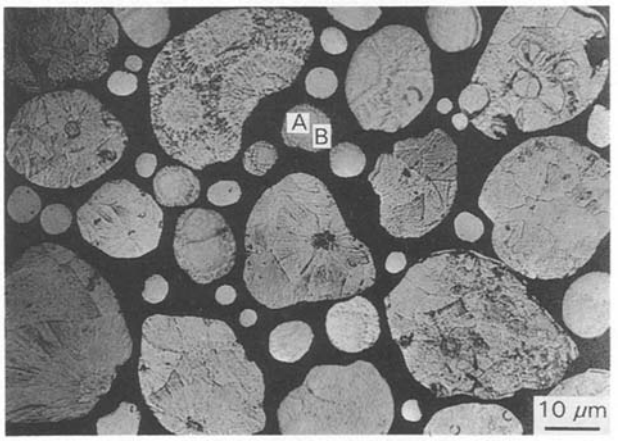

Figure 1 Optical micrograph of as-rapidly-solidified alloy powders. Note the presence of nucleants in large powder particles and the transition from zone A to zone B structures in small particles.

45-μm particle (Fig. 3a) was determined by EDX analysis as Al–21.55 wt % Fe–11.22 wt % Ni (Mo was not analysed) while the overall composition of the particle was determined as Al–8.34 wt % Fe–3.91 wt % Ni. Thus the Fe : Ni ratio of the τ phase is nearly the same as for the bulk alloy. By comparing the TEM and optical micrographs, it is concluded that the zone A structure in Fig. 1 is in fact microcellular structures (indicated as site 1 in Fig. 2), and the zone B structure consists of coarse cellular or eutectic structures.

3.2. Microstructure and properties of extrusions

XRD revealed that the extrusions contain only α-Al and τ phases, similar to the case of sub-200 μm powders, as shown in Table I. No evidence of the existence of Al–Mo or Al–Fe phases has been found in the extrusions. This is consistent with the phases found in the rapidly solidified powders.

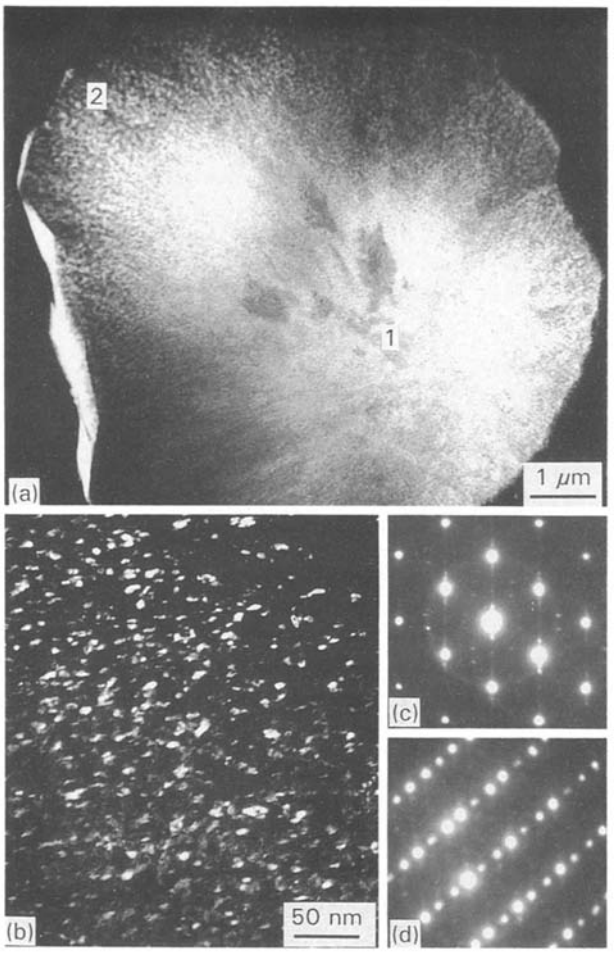

Figure 2 TEM image of a powder particle around 8 μm in diameter (a), dark-field image from site 1 with τ reflection (b), and SAD patterns at $[1\,1\,0]_{\alpha-Al}$ from site 1 (c) and site 2 (d).

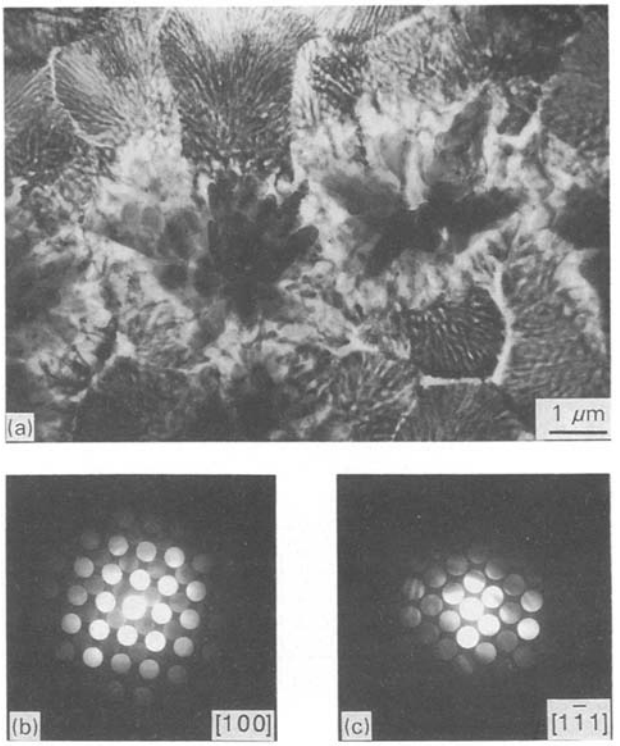

Figure 3 TEM image of a 45-μm powder particle (a) and CBED patterns (b) and (c) from the eutectic τ lathes.

Fig. 4a (extrusion A) and b (extrusion B) shows the general features of the alloy extrusions which are composed of alternating bands of coarser and finer structures; the coarser bands are generally much narrower than the majority finer region, and wider, coarser bands were observed in extrusions of larger extrusion ratio. Pores which can be expected at former powder particle boundaries were frequently found associated with the coarse band (Fig. 4a and b). Fig. 4c is a TEM dark-field image of the alloy extrusion A (the following TEM results are from extrusion A if not specified), showing the distribution of fine and coarse τ precipitates. Diffraction analysis showed that the coarse precipitates were always associated with large-angle grain boundaries, and the majority of the finer precipitates were generally at subgrain boundaries. By comparing with the SEM image shown in Fig. 4a, it is probable that the coarser bands are more likely to exist at the boundaries of powder particles, where both large-angle grain boundaries and pores are expected. The representative TEM microstructure of the finer region is shown in Fig. 4d, indicating a uniform distribution of τ particles in an aluminium matrix.

Some as-solidified powder particles were found to be retained in the extrusions (Fig. 5a and b). In these particles, the eutectic structure did not change while the microcellular structure underwent solid-state precipitation with a morphology very similar to that observed by Bendersky [9] and Kim & Jackson [11]. Diffraction analysis showed that the retained powder particle in Fig. 5b is composed of τ precipitates and a single crystal α-Al matrix, with close orientation relationship between the two phases. This relationship is shown in the superimposed SAD pattern in Fig. 5b, which reveals two equivalent orientation variants between α-Al and disk-shape τ, i.e. $\{1\,0\,0\}_\alpha//(1\,0\,0)_\tau$, which are typical orientation relationships reported by Kim & Jackson [11] and Bendersky [9]. Fig. 6 shows representative images of the same extrusion as shown in Fig. 4a, c and d (extrusion A) after being aged at 480 °C for 4 h. Comparing Fig. 6 with 4c and d, it is clear that τ is quite stable at 480 °C as the precipitate coarsening is quite modest.

Table II shows the effect of extrusion ratio on the mechanical properties of the alloy extrusions, indicating that higher extrusion ratio leads to poorer mechanical properties, particularly the yield strength.

4. Discussion

4.1. Powder microstructure

The only phases observed in the alloy powders were α-Al and τ, meaning that the separation of primary Al_3Fe to the ternary peritectic has been suppressed due to the metastable conditions obtainable under higher levels of undercooling in the powder particles from rapid solidification [14]. The observed extension of the line of binary separation between α-Al and τ to lower nickel levels is also in agreement with Perepezko's prediction [16]. The microcellular structures in small powder particles, as shown in Fig. 2, are believed to form under very large undercooling, while the primary τ and "α-Al + τ" eutectic structures form-

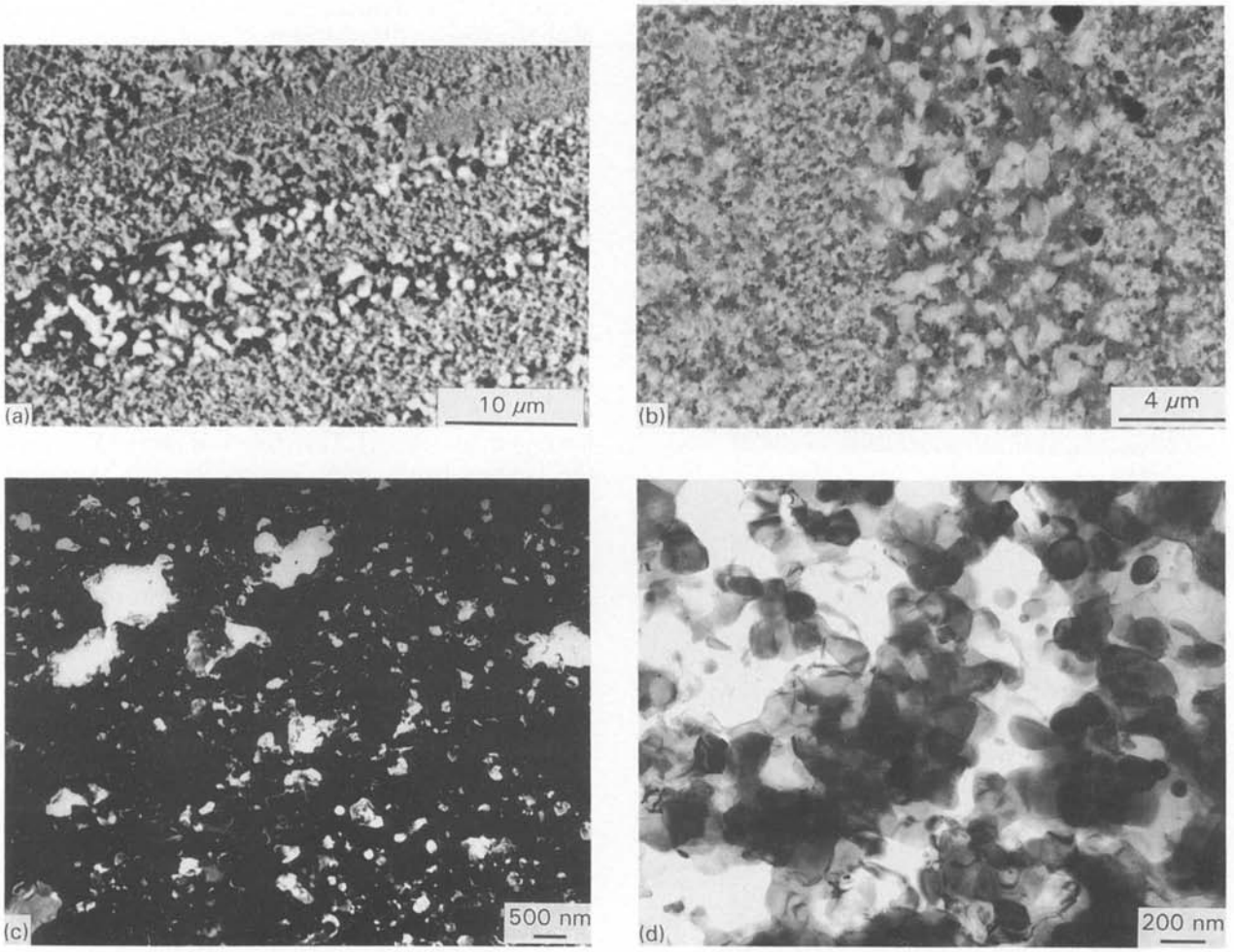

Figure 4 Back-scattered electron images of extrusion A (a, extrusion ratio 5:1) and B (b, extrusion ratio 27:1); (c) dark-field image using $(0\,1\,1)_\tau$ reflection (extrusion A); (d) representative TEM image of the majority fine region in extrusion A.

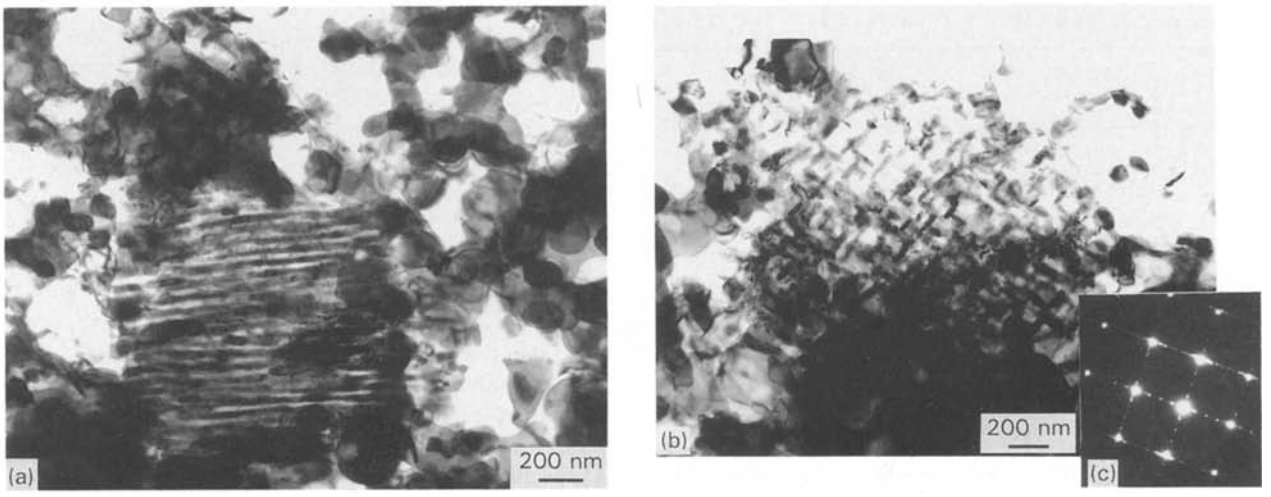

Figure 5 TEM images of the alloy extrusion: (a) eutectic structure in the powder particles retained in the extrusion (extrusion B); (b) fine powder particle retained in the extrusion (extrusion B) with solid-state τ precipitation; (c) SADP at $[1\,0\,0]_{Al}$ from (b), showing two equivalent orientation variants between α-Al and τ.

ed under a lower undercooling level. Detailed analysis of the microstructural development and phase selection in alloy powders during solidification has been reported elsewhere [12].

4.2. Microstructure development in consolidated material

By comparing the microstructure of (i) the as-solidified powder particles; (ii) the retained powder particles in the extrusions; and (iii) the general feature of the extrusions with different extrusion ratios, it can be deduced that the change of microstructure is mainly due to the deformation exerted during the extrusion process. Retained particles which underwent much less strain showed little change in morphology. The precipitates in the retained fine particles, as shown in

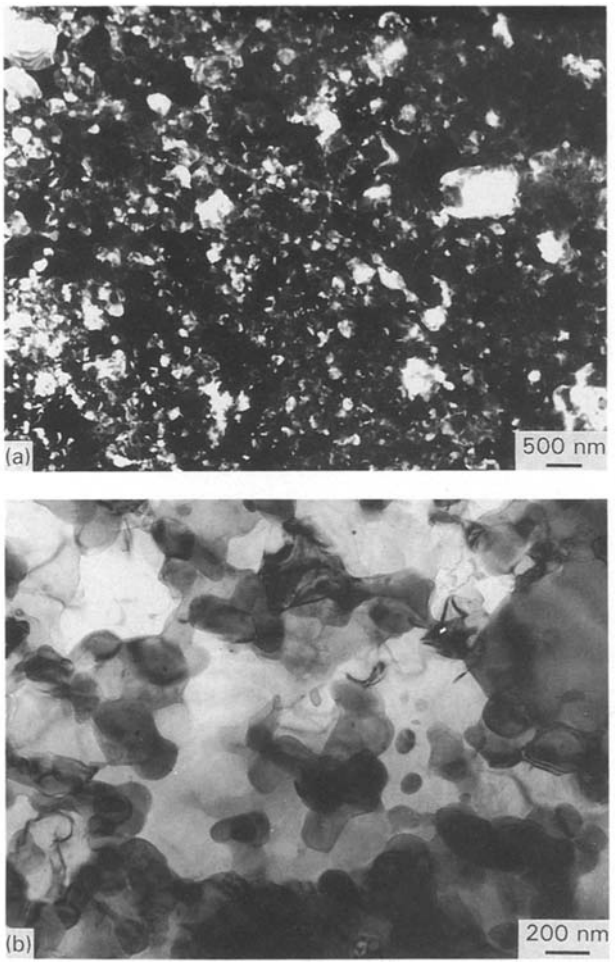

Figure 6 (a) Dark-field TEM image (using $(0\,1\,1)_\tau$ reflection) of the alloy extrusion (A, extrusion ratio 5:1) after ageing at 480 °C for 4 h.

TABLE II Mechanical properties of the alloy extrusions

Extrusion ratio	YS (MPa)	UTS (MPa)	El (%)
5:1	519	548	7
27:1	415	525	7

Fig. 5b, maintain a close orientation relationship with the single-crystal matrix, and the precipitate morphology is identical with that obtained by heat treatment. The eutectic structure in larger retained particles did not change morphology despite the same thermal exposure during extrusion. Also, coarser bands are wider when the extrusion ratio is larger. Finally, a heat treatment test of the alloy extrusion at 480 °C proved that τ was quite stable at the extrusion temperature. By contrast, all the coarser morphologies seem to be associated with features that are linked to prior particle boundaries where pores and large grain boundaries are expected. Therefore, it may be concluded that the severe plastic deformation exerted on the particles accelerated the rate of precipitate coarsening during recovery and recrystallization.

A banding phenomenon has also been observed in Al–Fe extrusions [15]. However, here the coarser precipitates were identified with primary Al_3Fe and finer ones were derived by transformation from Al_6Fe[14]. This mechanism cannot explain our results as τ precipitates in the rapid solidification powder are also the stable phase at extrusion and heat-treatment temperature [12, 14]. Banding has also been reported in Al–Fe–Ni alloys with Ni:Fe ratio around 1, where only τ and α-Al were observed in the rapid solidification materials [8]. Therefore it is more likely that the coarser bands were formed through enhanced diffusion rate associated with the higher energy present in regions of high strain concentration. It is expected that powder particle boundaries, which provide the bridge for energy transfer from particle to particle by axial pressing and lateral friction, are more likely to show high strain levels, especially the lateral boundaries. This will also give rise to local adiabatic heating and will lead to aluminium grains at the particle bonding regions containing a few large τ precipitates on large-angle grain boundaries with associated precipitate-depleted regions. The precipitate-depleted regions then form self-propagating bands through the rest of the extrusion. Regions of lower strain levels also underwent some coarsening, but with a much reduced rate.

TABLE III Effect of extrusion ratio on the mechanical properties of Al–8Fe–1Ni–1Cr–1Mo extrusions

Ratio	Temperature (°C)	YS (MPa)	UTS (MPa)	El (%)	K_{IC} (MPa $m^{1/2}$)
5:1	480	421	498	11	11
15:1	450	399	472	6	12
27:1	480	320	440	14	–

The coarser bands in the extrusions will provide weaker parts in the extrusions, leading to lower strength. Table III shows the effect of extrusion ratio on the mechanical properties of the extrusions of Al–8 wt % Fe–1 wt % Ni–1 wt % Cr–1 wt % Mo rapid solidification alloy powders, indicating the same trend of strength changes with extruding ratio [15]. This means that the effect reported here may be of general importance, suggesting the use of the lowest extrusion ratio that guarantees particle bonding.

5. Conclusions

Microstructural investigation of a rapidly solidified Al–Fe–Ni alloy showed that τ is quite stable when exposed at 480 °C. It is concluded that bands with coarse τ precipitates and thus large precipitate spacing only form in regions with higher strain levels, such as the prior particle boundaries. The mechanical properties of the extrusions were found to be related to the extent of banding and its associated precipitate distribution. A larger extrusion ratio appears to lead to more severe banding, and hence there should be a compromise between optimum powder bonding and lowest possible extrusion ratio in the consolidation process.

Acknowledgements

The authors thank Professor J. E. Castle for provision of laboratory facilities. One of the authors (G.S.) is grateful to the Chinese government and the British

Council for financial support. The materials being investigated formed part of Euram programme MA1E/0076/C for the development of higher strength aluminium alloys.

References

1. C. M. ADAM, V. R. V. RAMANAN and D. J. SKINNER, in "Undercooled Alloy Phases", edited by E. W. Collings and C. C. Coch, (Metals Society of AIME, 1987) p. 59.
2. M. DE SANCTIS, A. P. WOODFIELD and M. H. LORRETTO, *Int. J. Rapid Solidification* **4** (1988) 53.
3. I. R. HUGHES and H. JONES, *J. Mater. Sci.* **11** (1976) 1781.
4. G. VIGIER, U. ORTIZ-MENDEZ, P. MERK, G. THOLLET and F. FOUGUET, *Met. Sci. Engng* **98** (1988) 53.
5. W. J. BOETTINGER, L. BENDERSKY and J. G. EARLY, *Met. Trans* **17A** (1986) 781.
6. N. DUDZINSKI, *J. Inst. Metals* **83** (1955) 444.
7. M. K. PREMKUMAR, A. LAWLEY and M. J. KOCZZAK, in "Modern Development in Powder Metallurgy", edited by E. N. Aqua and C. I. Whiteman (Metal Powder Industries Federation, Princedon, New Jersey, 1985) p. 467.
8. M. K. PREMKUMAR, A. LAWLEY and M. J. KOCZZAK, *Met. Trans.* **23A** (1992) 3219.
9. L. BENDERSKY, *Met. Trans.* **16A** (1985) 683.
10. W. J. BOETTINGER, L. A. BENDERSKY, R. J. SHAEFER and F. S. BIANCANIELLO, *Met. Trans.* **19A** (1988) 1101.
11. Y. KIM and A. G. JACKSON, *Scripta Met.* **20** (1986) 777.
12. G. SHAO, P. TSAKIROPOULOS and A. P. MIODOWNIK, "The Microstructure of Rapidly Solidified Al–8Fe–4Ni–1Mo Alloy Powders", *Int. J. Rapid Solid.* (in press).
13. G. SCHARF, H. MCSHANE, P. SMITH and A. P. MIODOWNIK, EURAM Final Report Project MA1E/0076/C (1991).
14. A. P. MIODOWNIK, in Proceedings of the ASM Conference on Advanced Materials, (ICOMP), Bombay, February 1992 (in press).
15. M. STRANGWOOD, J. H. TWEED and R. M. K. YOUNG, *Mater. Sci. Engng.* **A134** (1991) 1148.
16. J. H. PEREPEZCO, in "Alloy Phase Diagrams" edited by L. H. Bennett, T. B. Massalski and B. C. Giessen (North Holland, New York, 1982) p. 223.

Received 12 August
and accepted 14 September 1993